EurJIC
European Journal of Inorganic Chemistry

Research Article
doi.org/10.1002/ejic.202200597

Chemistry Europe
European Chemical Societies Publishing

www.eurjic.org

Ruthenium Complexes of Rigid, Dianionic, Tetradentate N-Donor Ligands and their Potential as Catalysts for Water Oxidation

Sheida Rajabi,[a] Franziska Rüttger,[a] Jana Lücken,[a] Sebastian Dechert,[a] Michael John,[a] and Franc Meyer*[a]

Two mononuclear ruthenium(II) complexes based on dianionic $\{N_4\}$ ligands and with axial pyridines have been prepared and characterized crystallographically (**1**) or by 2D NMR spectroscopy using residual dipolar couplings (**2**). The $\{N_4\}$ ligands provide a constrained equatorial coordination with one large N–Ru–N angle, and additional non-coordinating N atoms in case of **2**. Their redox properties have been investigated (spectro)electrochemically, and their potential to serve as water oxidation catalysts has been probed using cerium ammonium nitrate (CAN) at pH 1.0. Complex **1** undergoes rapid degradation, likely via ligand oxidation, whereas **2** is more rugged and exhibits 80% efficiency in the Ce^{IV}-driven water oxidation, with a high initial turnover frequency (TOF_i) of $3.07\times10^{-2}\ s^{-1}$ (at 100 equiv. CAN). The initial rate of O_2 evolution exhibits 1st order dependence on catalyst concentration, suggesting a water nucleophilic attack mechanism. Repeated addition of CAN and control experiments show that high ionic strength conditions (both NO_3^- and Ce^{III}) significantly decrease the TOF.

Introduction

A sustainable energy supply of the future should use chemical fuels whose production is resource-conserving and environmentally friendly.[1–3] Artificial photosynthesis and the solar-driven generation of hydrogen from water are considered as a potential solution to lower the consumption of carbon-based fossil resources.[4–7] The oxidative half-reaction of water splitting, viz. the four-electron oxidation of water to dioxygen, is a key step in this context. However, this oxygen evolution reaction (OER) is thermodynamically and kinetically demanding, and it requires robust and powerful catalysts that can withstand harsh reaction conditions. Among molecular water oxidizing catalysts (WOCs), ruthenium-based systems are particularly prominent and exhibit the most promising catalytic performance. Extensive mechanistic studies have been performed for both mono- and dinuclear ruthenium WOCs[8–15] and have shown that the critical O–O bond formation may occur via coupling of two metal oxo units (I2 M) or nucleophilic attack of water onto a high valent Ru=O centers (WNA) depending on the design and electronic structure of the catalyst.[16–18] More recently, for complexes with non-coordinating N-atoms close to the active site, an alternative mechanism has been proposed where oxidizing equivalents are stored on the ligand via O-atom transfer (OAT) to generate an N–oxide group; O–O coupling then proceeds via the interaction of a high-valent Ru=O and the N–O unit.[19]

Over the last decades, impressive catalytic activities have been achieved with ruthenium-WOCs based on tetradentate (bda: type **A**)[20,21] or pentadentate (tda: type **B**)[12] ligands (Figure 1) in which oligopyridyl chelating scaffolds are equipped with peripheral carboxylate groups, and reaction pathways are tuned by modification of the axial ligands.[22,23] It has been shown that these complexes can form seven-coordinate $Ru–OH_x$ intermediates, and the metal reaches a high +V oxidation state;[24–26] oxidation at relatively low potentials is facilitated by the anionic carboxylate groups that lower the overall charge of the complexes. The bda-derived complexes usually follow the I2M mechanism while tda-based systems favor a WNA scenario assisted by the dangling carboxylate groups that serve as H-bond acceptors for the water nucleophile.[27–29] On the other hand, much efforts have been directed toward the immobilization of efficient WOCs on solid supports without compromising the stability and performance of the system.[30–33] To that end, type **A** and **B** complexes have been equipped with various anchoring groups for successful immobilization on carbonaceous surfaces,[31,34–36] but immobilization on metal oxide supports is complicated by the preferred interaction of the ligand carboxylates with the surface.

A family of topologically related ruthenium complexes bearing equatorial ligands with only N-donors, such as the tetradentate N4 ligands 2,2′:6′,2″:6″,2‴-quaterpyridine (qpy; type **C**; Figure 1)[37] or 2,2-(1,10-phenanthroline-2,9-diyl)bis(pyridine) (bpb; type **D**; Figure 1)[38,39] have been found to also serve as WOCs and to generate O_2 after treatment with an oxidant. However, due to their neutral N-donor ligands these

[a] Dr. S. Rajabi, F. Rüttger, Dr. J. Lücken, Dr. S. Dechert, Dr. M. John, Prof. Dr. F. Meyer
Georg-August-Universität Göttingen
Institut für Anorganische Chemie
Tammannstrasse 4, 37077 Göttingen, Germany
E-mail: franc.meyer@chemie.uni-goettingen.de
https://uni-goettingen.de/de/611271.html

Supporting information for this article is available on the WWW under https://doi.org/10.1002/ejic.202200597

Research Article
doi.org/10.1002/ejic.202200597

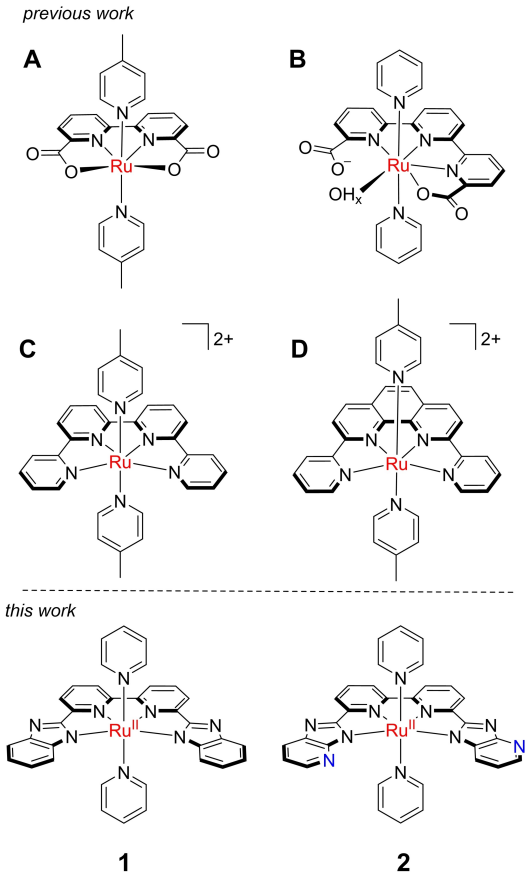

Figure 1. Previously reported mononuclear ruthenium water oxidation catalysts based on bda (**A**),[20] tda (**B**)[12] qpy (**C**),[37] and bpb (**D**)[38] ligand scaffolds (top and middle), and new complexes **1** and **2** reported in this work (bottom).

complexes are positively charged, which usually leads to higher redox potentials and often favors detrimental leaching of immobilized catalysts into an aqueous solution. During chemical water oxidation, the two catalysts **C** and **D** initially undergo ligand oxidation at the outer pyridyl rings to form the qpy/bpb-*N*,*N*′′′-dioxide (ONNO) ligands, and the resulting $[Ru(ONNO)(pic)_2]^{2+}$ complexes are considered as the actual and active WOCs.

With the aim of combing beneficial features of both classes of Ru-based WOCs **A**/**B** and **C**/**D** -viz., exploiting anionic ligand character but using N-donors only, in an overall complex topology similar to the above catalysts- we now introduce the two new ruthenium complexes **1** and **2** (Figure 1). Their synthesis and characterization are reported, as well as preliminary studies on their ability to serve as WOCs.

Results and Discussion

Synthesis and characterization of H_2L^2 and ruthenium complexes

Proligand $\mathbf{H_2L^1}$ was prepared following a previously reported protocol,[40,41] and $\mathbf{H_2L^2}$ was synthesized via a similar procedure using 2,2′-bipyridine-6,6′-dicarboxylic acid and 2,3-diaminopyridine, which were coupled under acidic condition (Scheme 1). The reaction of $\mathbf{H_2L^1}$ and $[RuCl_2(C_6H_6)]_2$ in presence of NEt_3 in degassed MeOH followed by the addition of an excess amount of pyridine leads to the formation of complex $[L^1Ru(py)_2]$ (**1**) as a brown solid. Complex $[L^2Ru(py)_2]$ (**2**) is obtained similarly, but using $RuCl_2(dmso)_4$ as the ruthenium precursor (Scheme 2).

Both complexes were purified by column chromatography, and in the case of **1** crystals suitable for X-ray diffraction could be grown by slow evaporation of a solution of the complex in chloroform. The molecular structure shown in Figure 2 confirms the expected constitution with $[\mathbf{L^1}]^{2-}$ serving as a dianionic tetradentate equatorial ligand and with pyridines in the axial positions, giving an $\{N_6\}$ coordination environment for the central Ru^{II} ion. The Ru–N bonds involving the inner pyridyl rings of $[\mathbf{L^1}]^{2-}$ (Ru1–N1 1.963 Å, Ru1–N2 1.967 Å) are significantly shorter than the Ru–N bonds involving the outer benzimidazolato groups (Ru1–N3 2.133 Å, Ru1–N4 2.145 Å), which is caused by the rigidity and the acute bite angles of the tetradentate ligand framework. As a result, the angle N3–Ru1–N4 (122.4°) is widened by 32° relative to the ideal octahedral geometry and much wider than all other N–Ru–N

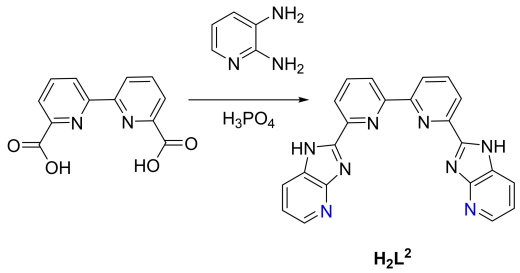

Scheme 1. Synthetic procedure for the preparation of $\mathbf{H_2L^2}$

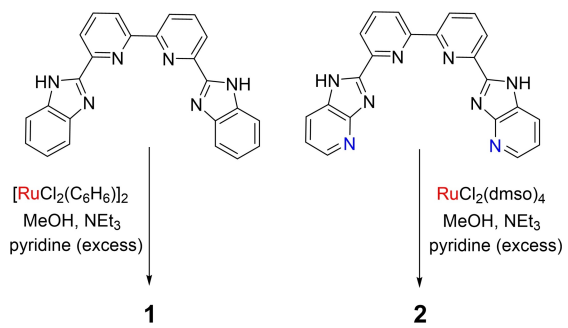

Scheme 2. Synthesis of complexes **1** and **2**.

Research Article
doi.org/10.1002/ejic.202200597

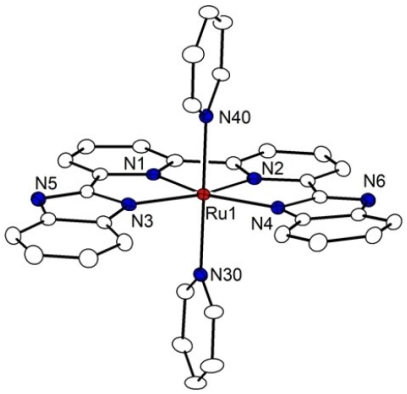

Figure 2. Molecular structure of **1**. For clarity, hydrogen atoms and solvent molecules have been omitted.

angles in **1**, possibly allowing a seventh ligand (such as water) to bind in the open cleft of the equatorial plane.

Both complexes have been characterized in solution by 1D and 2D NMR spectroscopy and electrospray ionization mass spectrometry (ESI(+)-MS; see Supporting Information). The ESI(+) mass spectrum in MeOH shows the expected protonated ion $[LRu(py)_2+H]^+$ at *m/z* 647.1 (**1**) and 649.2 (**2**) even after storing the MeOH solutions for longer times, indicating that the axial pyridine ligands are not substituted under those conditions. The ^{1}H NMR spectrum of **1** in MeOH-d_4 shows 10 distinct resonances in the region typical for aromatic groups, reflecting the C_{2V} symmetry of the complex. In case of **2**, however, 13 signals integrating to 22 protons are observed in that region (including some signal overlap; Figure S18), indicating a lower symmetry. To elucidate the structure of **2** in solution, residual dipolar couplings (RDCs) were measured in addition to conventional 2D-NMR methods.

The correlation between H-12 and H-10 in the ^{1}H-^{1}H NOESY spectrum of **2** (highlighted as green boxes in Figure 3) suggests the formation of an *in*, *out* isomer as the main product, where the two imidazo[4,5-*b*]pyridine units are oriented in the same direction. For residual dipolar couplings (RDCs) experiments, C–H coupling constants were measured using the CLIP-HSQC[42] on both an isotropic sample and an anisotropic sample in a swollen cross-linked polystyrene[43,44] from which the RDCs can be extracted (Figures S35 and S36). For these measurements, THF-d_8 was used as a solvent instead of MeOH-d_4 as methanol does not swell polystyrene. For the analysis of the RDCs, MSpin was used.[45] There, a list of RDCs assigned to the respective C–H groups is compared to theoretical RDCs of a structure model, which is in this case a geometry optimized structure calculated by Gaussian 16 (Figure 4 < A).[46] The difference between the experimental and the theoretical RDCs is expressed by a quality factor that indicates how well the RDCs and their assignment to particular C–H groups fit the structure.[47] Thus, a proposed structure can be confirmed while all the signals can be safely assigned in the respective solvent used. In the case of complex **2**, the theoretical RDCs fit excellently with the experimental values (Figure 4B), which confirms the structure model of an *in*, *out* isomer with a quality factor of 0.04. Notably, even the signals of the bipyridine unit, for which there is no external connectivity information, could be assigned this way (Figure S37); an assignment with the groups 2–4 and 2′-4′ swapped leads to a much poorer agreement of experimental and theoretical RDCs with a quality factor of 0.23.

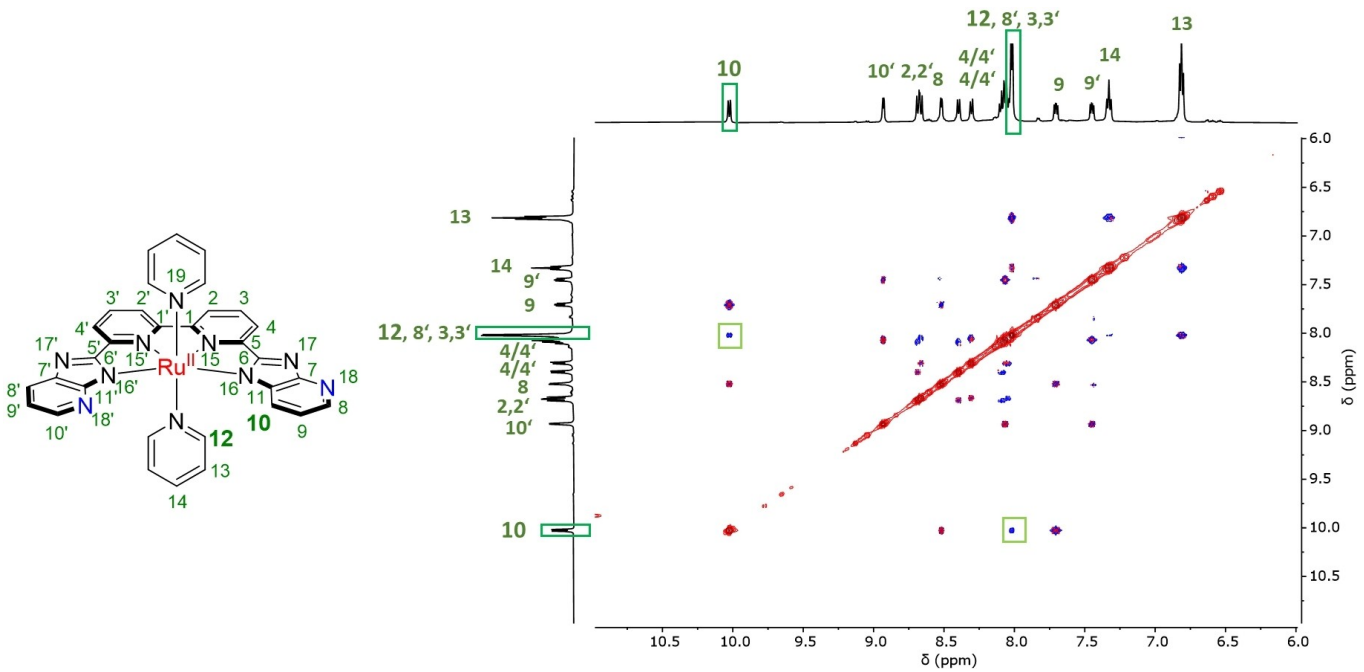

Figure 3. ^{1}H-^{1}H-NOESY spectrum of complex **2** in MeOH-d_4 at room temperature. The correlation between H-12 and H-10 is highlighted with green boxes.

Research Article
doi.org/10.1002/ejic.202200597

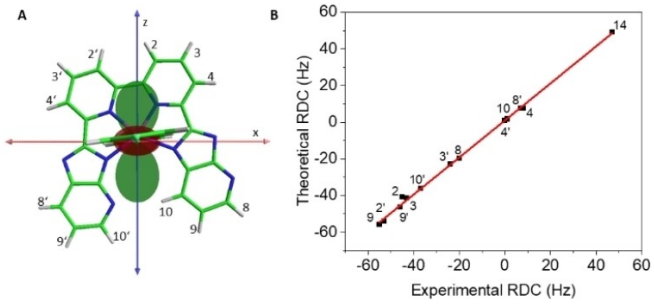

Figure 4. Calculated structure model of **2** showing the preferred orientation in oriented solution along the z-axis and the least preferred orientations along the y-axis (**A**). The theoretical RDC for the C–H groups of complex **2** plotted against the experimental RDC of each C–H group, respectively (**B**).

The reasons for the isolation of only the *in*, *out* isomer of **2** remain unclear. It may be speculated that formation of **2** is preferred because of the highly polar conditions used for its synthesis (MeOH solvent, excess NEt_3 and pyridine), favouring a higher dipole moment of the product. However, the yield of pure **2** isolated after column chromatography is rather low, and it may well be that other isomers are formed as well but are lost during workup.

Protonation studies

Since chemical water oxidation studies are performed under low pH conditions (0.10 M aqueous triflic acid; vide infra), the potential protonation of **1** and **2** and the stability of the complexes in acidic environment were investigated. To that end, titrations of MeOH solutions of **1** and **2** with aqueous HOTf were monitored by UV-vis spectroscopy (Figure 5). Upon the addition of acid, the characteristic intense absorption of **1** and **2** around 380 nm (tentatively attributed to metal-to-ligand charge transfer, MLCT) gradually decreases, and two new bands arise at slightly higher energy (350 and 362 nm); no further changes are observed after the addition of two equivalents of acid, indicating that twofold protonation is possible (inset Figure 5). Subsequent addition of base (1,5,7-triazabicyclo[4.4.0]dec-5-ene; TBD) fully recovers the original spectra of **1** and **2**, suggesting good stability of the protonated complexes. The in situ generation of protonated species $[\mathbf{1}H_2]^{2+}$ and $[\mathbf{2}H_2]^{2+}$ was also confirmed by NMR spectroscopy, which furthermore showed that protonation of the imidazo[4,5-*b*]pyridine units of **2** occurs at the peripheral N-atoms of the 5-membered rings (not the 6-membered rings; see Supporting Information).

For complex **1**, single crystals of $[\mathbf{1}H]PF_6$ and $[\mathbf{1}H_2](CF_3SO_3)_2$ were obtained by treating solutions of the complexes in CH_2Cl_2 with HPF_6 or CF_3SO_3H, respectively, and subsequent slow diffusion of diethyl ether into solutions of the crude products in MeOH. X-ray diffraction analyses confirmed protonation at the peripheral N atoms of the benzimidazole groups (Figure 6); the N-bound H atoms could be located and are found to H-bond to the respective anion. Ru–N bonds involving the equatorial tetradentate ligand undergo only minor changes compared to

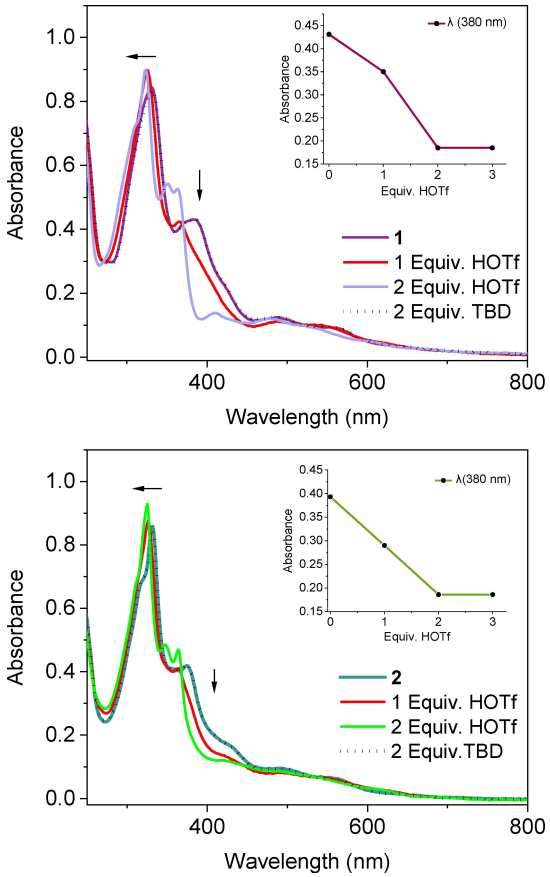

Figure 5. UV-vis titration of **1** (top) and **2** (bottom) with aqueous HOTf and TBD in methanol at room temperature.

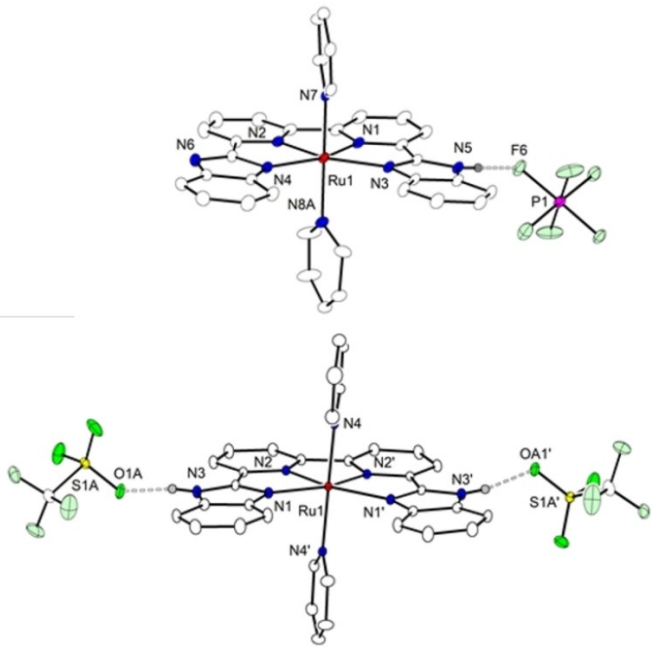

Figure 6. Molecular structures of $[\mathbf{1}H]PF_6$ and $[\mathbf{1}H_2](CF_3SO_3)_2$. Most hydrogen atoms (except the N–H) and disorders have been omitted for clarity.

Research Article
doi.org/10.1002/ejic.202200597

the parent neutral complex **1**; elongation is most pronounced for the Ru–N^{imid} bonds involving the benzimidazole–N (~0.03 Å) in line with protonation at those moieties (see Table 1). Also the wide angles N3–Ru1–N4 in [**1**H]PF_6 (123.5°) and N1–Ru1–N1′ in [**1**H_2]$(CF_3SO_3)_2$ (123.2°) are essentially unchanged (33°; versus 32° in **1**), indicating that the deviation from ideal octahedral geometry and the presence of a potentially accessible seventh coordination site remain under acidic conditions.

Electrochemical properties

The redox properties of complexes **1** and **2** were investigated in a 1:1 mixture of aqueous CF_3SO_3H (0.10 M, pH = 1.0) and 2,2,2-trifluoroethanol (TFE) using cyclic voltammetry (CV) and square wave voltammetry (SWV); as shown above, protonated species $[\mathbf{1}H_2]^{2+}$ and $[\mathbf{2}H_2]^{2+}$ are present under those conditions. ^{1}H NMR spectroscopy confirmed that $[\mathbf{2}H_2]^{2+}$ is stable in that solvent mixture for at least 48 h, without signs of loss of axial pyridines. Redox waves at $E_{1/2}$ = 1.23 V ($[\mathbf{1}H_2]^{2+}$) and $E_{1/2}$ = 1.16 V ($[\mathbf{2}H_2]^{2+}$; all potentials vs. RHE) are assigned to the reversible one-electron Ru^{III}/Ru^{II} couple; oxidation to the Ru^{III} species is slightly more facile for $[\mathbf{2}H_2]^{2+}$ whose {N_4} ligand [$H_2\mathbf{L}^2$] is less e^--donating. At higher potentials both complexes feature an electrocatalytic current (E_{onset} is around 1.5 V for $[\mathbf{1}H_2]^{2+}$ and 1.4 V for $[\mathbf{2}H_2]^{2+}$; Figure 7).

Chemical reversibility of the Ru^{III}/Ru^{II} redox process was further studied by UV/vis-spectroelectrochemistry in a 1:1 mixture of aqueous HOTf (0.10 M, pH = 1.0) and TFE (Figure S40). Initial spectra are similar to those observed for protonated species $[\mathbf{1}H_2]^{2+}$ and $[\mathbf{2}H_2]^{2+}$ in the titration experiments, cf. Figure 5. Upon oxidation at 1.35 V ($[\mathbf{1}H_2]^{2+}$) or 1.25 V ($[\mathbf{2}H_2]^{2+}$) vs. RHE, the intensity of the bands at 320, 346, and 362 nm slightly decreases and the broad band at 480 nm vanishes after conversion to the Ru^{III} species. The original spectra of $[\mathbf{1}H_2]^{2+}$ and $[\mathbf{2}H_2]^{2+}$ are fully recovered after electrochemical re-reduction at 1.10 V or 1.12 V, respectively. To further quantify the variation of the band intensity at 480 nm, and to ascertain that the same spectral changes occur upon chemical oxidation, a concentrated solution (10^{-3} M) of $[\mathbf{2}H_2]^{2+}$ was titrated with cerium(IV) ammonium nitrate (CAN) up to the addition of 1 equiv. (Figure 8). Spectral signatures for the electrochemical and chemical oxidation processes indeed show good agreement.

To examine the ruggedness of the complexes at high potentials under catalytic conditions, repetitive CV scans were carried out, cycling the potential range 0.80–1.83 V *vs.* RHE at a scan rate of 50 mV/s (Figure 9). A considerable decrease of the electrocatalytic current as well as a decrease of the wave for the Ru^{III}/Ru^{II} couple are observed in case of $[\mathbf{1}H_2]^{2+}$, indicating gradual decomposition of the complex on the time scale of the

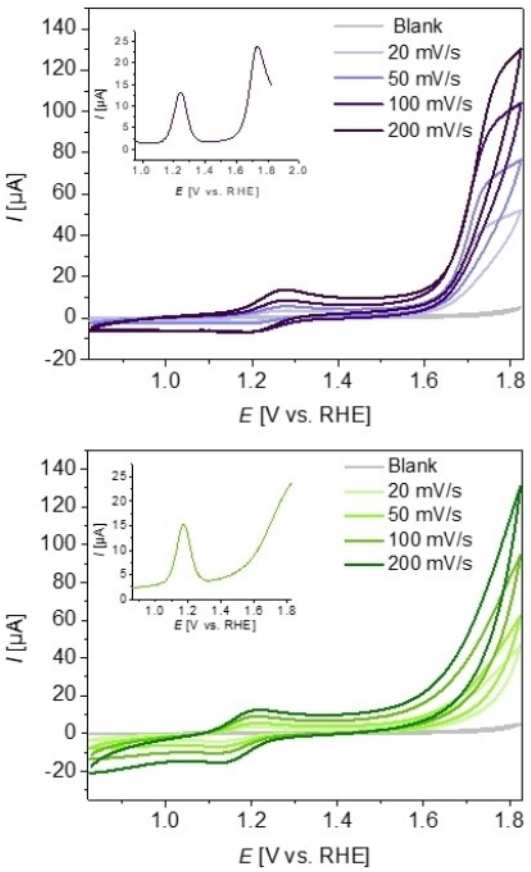

Figure 7. Cyclic voltammetry of **1** (top) and **2** (bottom) in a 1:1 mixture of aqueous triflic acid (0.10 M, pH = 1.0) and TFE at different scan rates using glassy carbon as a working electrode, platinum as a counter electrode, and MSE as a reference electrode (complex concentration: 10^{-3} M); blank measurements recorded under the same conditions (solid grey). The insets show the corresponding SWVs. All potentials are referenced versus the RHE scale.

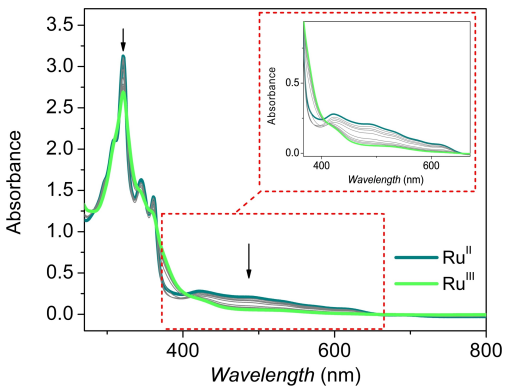

Figure 8. UV/vis spectra for the chemical oxidation of $[\mathbf{2}H_2]^{2+}$ from Ru^{II} (dark green) to Ru^{III} (light green) upon titration with CAN in steps of 0.10 equiv., up to 1 equiv..

Table 1. Selected distances [Å] and angles [°].

	1	[**1**H]PF_6	[**1**H_2]$(CF_3SO_3)_2$
Ru–N^{bipy}	1.963(3)/1.967(3)	1.9545(16)/1.9629(15)	1.959(3)
Ru–N^{imid}	2.133(3)/2.145(3)	2.1581(15)/2.1791(15)	2.169(3)
Ru–N^{py}	2.086(3)/2.092(3)	2.0838(15)/2.1085(17)	2.096(3)
N^{bipy}–Ru–N^{bipy}	80.43(14)	80.21(7)	80.45(16)
N^{imid}–Ru–N^{imid}	122.42(13)	123.54(6)	123.15(15)
N^{py}–Ru–N^{py}	175.37(13)	175.91(6)	174.2(2)

Research Article
doi.org/10.1002/ejic.202200597

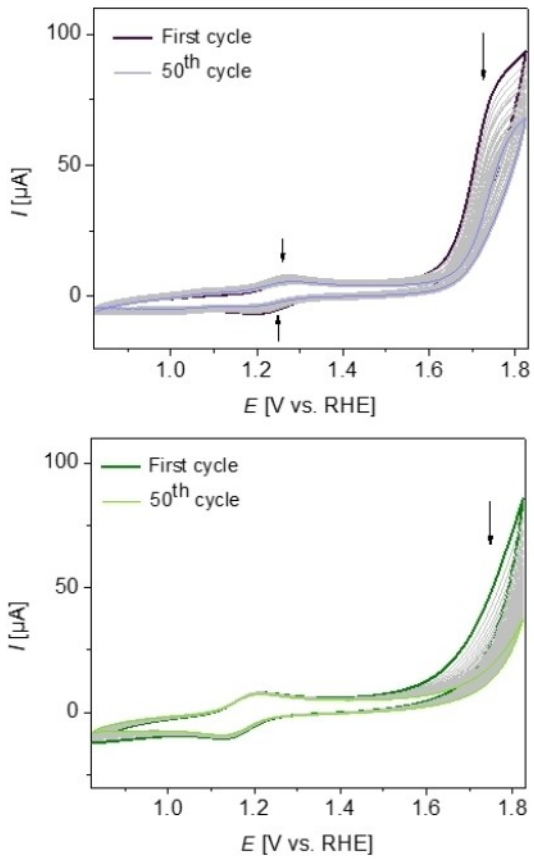

Figure 9. Repetitively measured CVs of complexes $[\mathbf{1}H_2]^{2+}$ and $[\mathbf{2}H_2]^{2+}$ in a 1:1 mixture of aqueous triflic acid (0.10 M, pH = 1.0) and TFE at a scan rate of 50 mV/s within the range 0.80–1.83 V *vs.* RHE. WE: glassy carbon, CE: platinum, Ref: MSE.

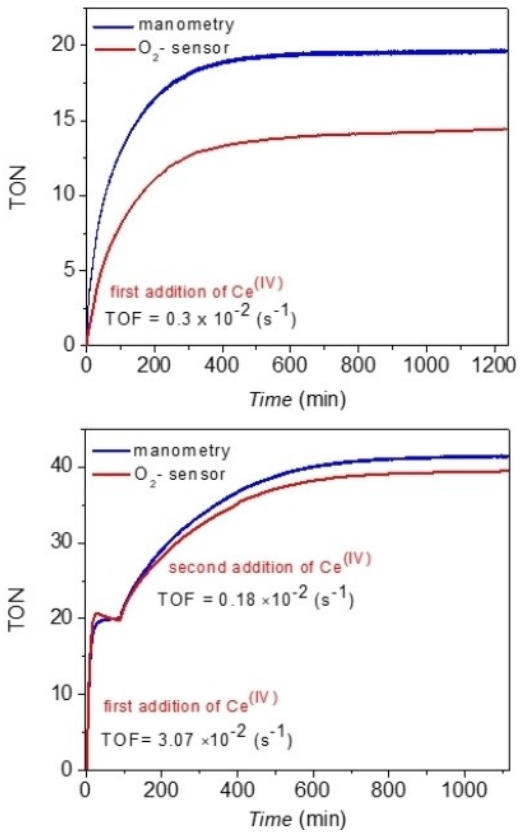

Figure 10. Chemically driven water oxidation catalysis of **1** (top) and **2** (bottom) upon addition of CAN into a solution of the complex in an aqueous triflic acid solution (0.10 M, pH = 1.0) at 25 °C. The oxygen evolution is monitored simultaneously by on-line manometry (blue) and optical oxygen sensor (red).

experiment. Complex $[\mathbf{2}H_2]^{2+}$ exhibits higher stability judged by the unchanged wave for Ru^{III}/Ru^{II} couple, but also displays a continuous decrease in electrocatalytic current.

Water oxidation catalysis with Ce^{IV} as a chemical oxidant

The potential of both **1** and **2** to serve as catalysts for chemically driven water oxidation has been studied using CAN as a sacrificial oxidant under acidic conditions. Catalysis is initiated by the addition of 100 equiv. of CAN to a 1 mM solution of the complex in aqueous triflic acid (0.10 M, pH = 1.0); thus the formation of 25 equiv. of O_2 (TON 25) would correspond to an efficiency of 100%. In these experiments, gas evolution was recorded simultaneously by online manometry and an optical oxygen sensor, and comparison of the two data sets provides information on whether gases other than O_2 are generated.

Complex **1** (present as $[\mathbf{1}H_2]^{2+}$ at pH 1.0) shows a significant gap between the manometry (blue) and oxygen sensor (red) readings after the first addition of 100 equiv. CAN, suggesting the production of other gases during the catalysis (Figure 10, top). Hence the headspace of the reaction cell was analysed by GC-MS, which showed the presence of significant amounts of CO_2 (Figure S41). It is thus likely that oxidative degradation of the ligand to CO_2 occurs under harsh WOC conditions, in agreement with the instability of $[\mathbf{1}H_2]^{2+}$ found at high electrochemical potentials. Hence, WOC with **1** was not investigated any further.

In contrast, complex **2** (present as $[\mathbf{2}H_2]^{2+}$ at pH 1.0) reaches a TON of around 20, corresponding to a good efficiency of 80% under identical conditions (100 equiv. of CAN in 0.10 M aqueous HOTf at 25 °C). Manometry and oxygen sensor measurements are in very good agreement (Figure 10, bottom), indicating that O_2 is the only gas produced during catalysis. Furthermore, the reaction is fast with a rather high initial turnover frequency (TOF_i) of $3.07\times10^{-2}\ s^{-1}$, which compares favourably with the value reported for **C** ($2.5\times10^{-2}\ s^{-1}$;[37] note that 100-fold higher excess of CAN has been used in the latter case, viz. 10.000 equiv.). TOF_i values for **2** are similar to those of some active pyrazolate-bridged diruthenium WOCs featuring solely N-donor ligands (1×10^{-2}–$7\times10^{-2}\ s^{-1}$), which have been studied under identical conditions (see Table 2).[17,48]

The chemical stability and activity of **2** was further investigated by adding further 100 equiv. of the oxidant CAN at the end of the first experiment, resulting in an overall TON of

Table 2. Catalytic data for **1**, **2**, **C** and a series of pyrazolate-bridged diruthenium WOCs containing N-donor ligands. 10.000 equiv. of CAN has been used in case of **C**.

Complex	TON (equiv. CAN)	TOF_i [s^{-1}]	ref
1	14.1 (100)	0.3×10^{-2}	this work
2	20.0 (100)	3.07×10^{-2}	this work
C	576 (10.000)	2.5×10^{-2}	37
pyrazolate-based Ru_2 complexes	17.0–22.6 (100)	1×10^{-2}–7×10^{-2}	17, 48

39 (efficiency of 76%; Figure 10, bottom). Good agreement between manometry and oxygen sensor readings suggests that the catalyst remains intact after the first run. However, the TOF_i is much lower in the second run (0.18×10^{-2} s^{-1}), which may be explained by the presence of large amounts of free nitrate and/or Ce^{III} ions originating from the CAN oxidant. Anation by nitrate (which competes with water for the active coordination sites)[49–51] or interaction of the catalyst with Ce^{III} have previously been reported for several ruthenium-based WOCs. When 200 equiv. of CAN are added to a freshly prepared solution of **2**, initially the manometry trace for O_2 evolution is similar to the one for the first run using 100 equiv. CAN up to a TON of 20, but the reaction rate then decreases as well (Figure S42). In order to probe the effect of NO_3^- and Ce^{III} ions on the rate of catalysis, the water oxidation experiment was conducted in the presence of 600 equiv. $NaNO_3$, 100 equiv. $Ce(NO_3)_3$ or a combination of both (viz. 300 equiv. $NaNO_3$ + 100 equiv. $Ce(NO_3)_3$) to emulate the ionic strength conditions with respect to NO_3^- or/and Ce^{III} resulting after completion of a catalytic first run with 100 equiv. of CAN. The findings presented in Figure S42 show that both, the addition of $NaNO_3$ or $Ce(NO_3)_3$ prior to water oxidation initiated by CAN, leads to significantly lower TOFs and deceleration of catalysis. Also, the active catalyst's concentration might gradually decrease due to the dissociation of the axial pyridine ligands at high Ru oxidation states, which could reduce the reaction rate, particularly in the second run. Hence the slowdown of water oxidation over the time scale of the experiment, or upon repeated addition of CAN, can be attributed, at least in part, to the change in the solution composition during the time scale of the WOC experiment.

Figure 11 (top) shows the time dependence of O_2 evolution for differing amounts of catalyst **2** ranging from 0.37–1.77 mM, while maintaining the CAN concentration at 100 mM. No initiation phase is discernible, and the initial rate of O_2 formation for each catalyst concentration is obtained from a linear fit to the O_2 evolution traces for the first 80 s (see inset). A first-order behaviour with respect to the catalyst indicates a mononuclear mechanism, likely operating via WNA for O–O bond formation. It may be speculated that the non-coordinating N-atom of the *in*-positioned imidazo[4,5-*b*]pyridine moiety in **2** may H-bond to incoming water and thus assist a WNA mechanism at a high-valent Ru=O intermediate.[52,53]

To gain information about the complex species present in solution after catalysis, solutions of **2** in a 1:1 mixture of 0.10 M triflic acid (pH 1.0) and TFE (viz., conditions as above) were

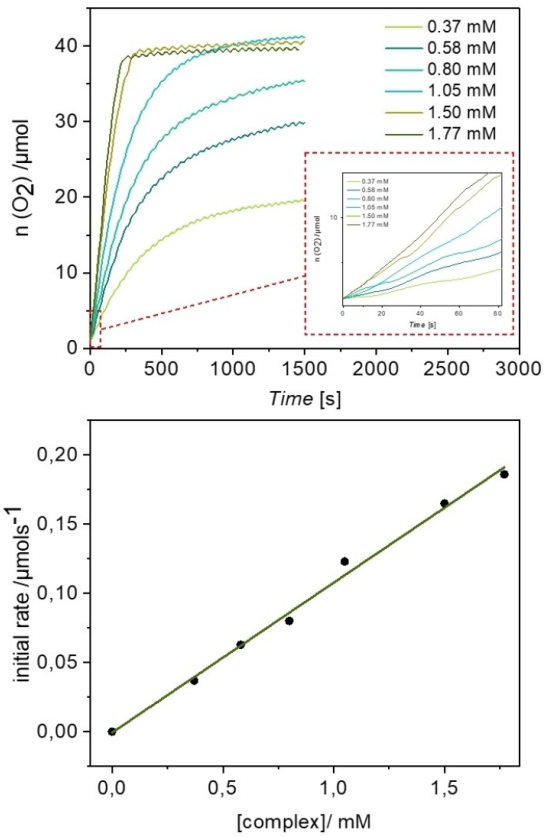

Figure 11. Top: O_2 formation measured by manometry at indicated concentrations of complex **2** and constant CAN concentration (100 mM); the inset shows the first 80 s of all experiments. Bottom: initial rate of O_2 formation (from the first 80 s of catalysis) vs. complex concentration.

treated with 30 equiv. CAN, and ESI(+) mass spectra were then recorded. A dominant peak at $m/z = 490.1$ (Figure S6) can be assigned to the ion $[L^2Ru+H]^+$, which suggests that the tetradentate $\{N_4\}$ ligand remains intact and bound to Ru, but that the axial pyridine ligands are lost during catalytic water oxidation. Therefore, the site of substrate (H_2O) binding and the exact identity of the catalytically active species remain unclear. The ESI(+) MS experiments do not provide any evidence for species containing an *N*-oxygenated ligand $\{L^2O_x\}$, in contrast to what was reported for catalysts **C** and **D**.

Summary and Conclusions

In this contribution we present two new ruthenium complexes **1** and **2** that have been designed to combine key features of active mononuclear ruthenium WOCs **A**/**B** and **C**/**D**, namely (i) a constrained tetradentate ligand scaffold that potentially allows for water coordination in the equatorial plane, (ii) dianionic character of the equatorial ligand scaffold to reduce the complexes' charge and overpotential like in **A**/**B**, and (iii) a ligand scaffold providing N-donors only, devoid of carboxylate groups, to prevent unwanted interactions with metal oxide surfaces upon immobilization. Furthermore, it was anticipated

that the additional N-atoms in the imidazo[4,5-*b*]pyridine groups of **2** might be able to serve as H-bond acceptor sites and water shuttles, akin the carboxylate groups in **A**/**B**. The structure of **1** was authenticated crystallographically. For **2**, based on detailed 2D NMR spectroscopic studies and using residual dipolar couplings it was shown that the isolated complex is the *in,-out* isomer. Both complexes **1** and **2** can be protonated twice at the peripheral imidazole-type N atoms to give $[\mathbf{1}H_2]^{2+}$ and $[\mathbf{2}H_2]^{2+}$, respectively, under acidic conditions. Electrochemical analyses evidence a reversible redox process at $E_{1/2} = 1.23$ V (for $[\mathbf{1}H_2]^{2+}$) or 1.16 V (for $[\mathbf{2}H_2]^{2+}$) vs. RHE and a large catalytic current above the onset potential. However, scanning to high potentials in repetitive CV measurements indicates that **1** is not stable under the harsh conditions of water oxidation; **2** appears to feature significantly higher stability within the applied potential range. The performance in chemically driven WOC was studied using CAN as a sacrificial oxidant at pH 1.0. In agreement with the electrochemical results, complex **1** is found to gradually degrade upon the addition of CAN under catalytic conditions, and the formation of CO_2 gas (likely originating from ligand degradation) was confirmed by GC-MS analysis. In contrast, complex **2** appears to be significantly more robust, though ESI-MS data recorded after CAN-driven WOC indicate the loss of the axial pyridine ligands. Therefore, chemical anchors for surface immobilization would likely have to be attached to the equatorial ligand scaffold. **2** features a first-order dependence of the initial rate of O_2 evolution on catalyst concentration, suggesting that a water nucleophilic attack mechanism (WNA) is operative. No evidence for *N*-oxygenation of the non-coordinating N-atoms of the imidazo[4,5-*b*]pyridine units in **2** was found, and hence the involvement of OAT transfer via N–O group (similar to what was reported for **C** and **D**[37,38]) seems unlikely. The beneficial role of the additional non-coordinating N-atoms in **2**, if compared with **1**, thus remains unclear, but one may speculate that the *in*-positioned N-atom could possibly serve as a water shuttle. Unfortunately, further experimental mechanistic investigations such as ^{18}O labelling experiments were hampered by the poor solubility of the complexes in aqueous solution.

Experimental Section

Materials and Methods

6,6′-bis-(1*H*-benzimidazol-2-yl)-2,2′-bipyridine ($\mathbf{H_2L^1}$)[40] and $RuCl_2(dmso)_4$[54] were prepared according to protocols reported in literature. Other reagents and solvents were purchased from commercial sources. Solvents were degassed before use, and all reactions were carried out under dried N_2 using Schlenk line techniques.

^1H, ^{13}C and ^{15}N NMR spectra were recorded on Bruker Avance III HD (AV400 MHz) and Bruker Avance III (500 MHz) spectrometers in MeOH-d_4. ^1H and ^{13}C chemical shifts were referenced to the residual solvent signal ($\delta(^1H) = 3.31$ ppm, $\delta(^1H) = 4.87$ ppm, $\delta(^{13}C) = 49.00$ ppm), ^{15}N chemical shifts were referenced relative to nitromethane. In case of the residual dipolar coupling measurements, THF was used as a solvent.

Electrospray ionization mass spectrometry (ESI-MS) was measured with a Finnigan MAT LCQ mass spectrometer.

Cyclic voltammetry (CV) and Square Wave Voltammetry (SWV) were performed with a Gamry interface (1010E) instrument using a three-electrode set-up: glassy carbon as a working electrode, platinum as a counter electrode, and MSE (mercury-mercurous sulfate electrode) as a reference electrode. All final potentials were reported vs. the RHE scale (reversible hydrogen electrode) using a conversion factor of 0.64 V. The working electrode was cleaned before the experiment by polishing it with alumina paste, and was then dried. All electrochemical measurements were carried out in a 1:1 mixture of 0.10 M aqueous triflic acid (pH 1.0) and TFE; TFE was used to increase the solubility.

UV-vis spectroelectrochemistry (SEC) experiments were conducted using a quartz cell with Pt mesh as a working electrode, Pt wire as a counter electrode and MSE as a reference electrode in a mixed solution of aqueous triflic acid (0.10 M, pH 1.0) and TFE (1:1). A Metrohm Autolab PGSTAT101 potentiostat was used, and UV-vis spectra were recorded with an Avantes AvaSpec-ULS2048L-StarLine spectrometer and Avantes AvaLight-DH-S-BAL light source.

Chemical water oxidation experiments were performed in home-made cells with a volume of 16.5 mL, and the temperature was kept constant (25 °C) during the catalysis. Two cells were tightly closed with a septum. Gas evolution was monitored simultaneously with online manometry with a differential pressure manometer (Testo 521-1) which was connected to a reference cell of nearly the same size and a gas phase oxygen sensor (OXF900PT) which was pierced through the septum of the reaction cell. The calibration before each experiment was performed with a two-point calibration in air and N_2-atmosphere. For the experiment, the cell containing the complex was degassed with N_2 for some minutes and then 1.85 mL of degassed 0.10 M triflic acid (pH 1.0) was added to both cells. After reaching the equilibrium between the reaction and reference cell, 150 μL of aqueous triflic acid (pH 1.0) was added to the reference cell, while 150 μL of a degassed solution of CAN in aqueous HOTf (pH 1.0) with a concentration of 10^{-3} M was added to the measurement cell.

Ligand and Complexes synthesis

Synthesis of H_2L^2

A mixture of 2,3-diaminopyridine (1.2 g, 10.56 mmol) and 2,2′-bipyridine-6,6′-dicarboxylic acid (1.19 g, 4.8 mmol) in phosphoric acid syrup (8 mL) was heated to reflux at 200 °C for 5 h. After cooling to room temperature, the solution was poured into ice and the formed precipitate was separated by filtration. The crude product was suspended in water and neutralized with 25% aqueous ammonia to give a slightly basic pH. The product was obtained as a purple solid after filtration and washing several times with water (yield: 67%).

^1H-NMR (500.3 MHz, MeOH-d_4 + NaOH): δ [ppm] = 8.38 (dd, J = 7.8, 0.8 Hz, 2H, bpy-H), 8.20 (dd, J = 4.8, 1.6 Hz, 2H, Ar–H), 8.11 (dd, J = 8.0, 0.9 Hz, 2H, bpy-H), 7.98 (t, J = 7.8 Hz, 2H, bpy-H), 7.97 (d, J = 7.9 Hz, 2H, Ar–H), 7.02 (dd, J = 7.8, 4.8 Hz, 2H, Ar–H).

^{13}C-NMR (125.8 MHz, MeOH-d_4 + NaOH): δ [ppm] = 163.7 (2 C, imidazole–C), 161.1 (2 C, imidazole, Ar–C), 155.5 (2 C, bpy–C), 155.3 (2 C, bpy–C), 142.2 (2 C, Ar–C), 140.5 (2 C, imidazole, Ar–C), 139.5 (2 C, bpy–C), 125.6 (2 C, Ar–C), 122.8 (2 C, bpy–C), 121.3 (2 C, bpy–C), 116.4 (2 C, Ar–C).

^{15}N-NMR (50.7 MHz, MeOH-d_4 + NaOH): δ [ppm] = −159.9 (4 N, imidazole–N), −114.8 (2 N, Ar–N), −89.3 (2 N, bpy–N).

MS (ESI+; MeOH): *m/z* (%) = 391.5 (100) $[M+H]^+$, 413.1 (95) $[M+Na]^+$.

Synthesis of Complex 1

A solution of $\mathbf{H_2L^1}$ (300 mg, 0.77 mmol), $[RuCl_2(C_6H_6)]_2$ (197 mg, 0.4 mmol) and NEt_3 (1 mL) in degassed methanol (20 mL) was heated to reflux under N_2 atmosphere for 1 day. Then, pyridine (1.4 mL) was added and the reaction mixture heated for another day. After cooling to rt, the resulting brown solution was filtered off and the solvent was removed under reduced pressure. The resulting brown crude product was purified by column chromatography (DCM/MeOH 100:2); brown complex **1** was obtained in 30% yield. Single crystals suitable for X-ray diffraction were obtained by slow evaporation of a solution of the complex in $CHCl_3$.

^{1}H-NMR (500.3 MHz, MeOH-d_4): δ [ppm] = 8.72 (d, J = 8.2 Hz, 2H, Ar–H), 8.59 (dd, J = 8.1, 1.0 Hz, 2H, bpy–H), 8.30 (dd, J = 8.0, 1.0 Hz, 2H, bpy–H), 8.06 (t, J = 8.0 Hz, 2H, bpy–H), 7.87 (dd, J = 5.2, 1.5 Hz, 4H, py–H), 7.73 (d, J = 8.1 Hz, 2H, Ar–H), 7.68 (ddd, J = 8.2, 7.1, 1.1 Hz 2H, Ar–H), 7.46 (ddd, J = 8.1, 7.1, 1.0 Hz, 2H, Ar–H), 7.36 (tt, J = 7.6, 1.6 Hz, 2H, py–H), 6.85 (m, 4H, py–H).

^{13}C-NMR (125.8 MHz, MeOH-d_4): δ [ppm] = 161.2 (Ph–C), 158.9 (imidazole–C),156.3 (bpy–C), 153.4 (py–C),143.4 (Ph–C), 142.5 (Ph–C), 137.9 (py–C), 135.5 (bpy–C), 125.9 (py–C), 125.3 (Ph–C), 124.8 (Ph–C), 123.6 (bpy–C), 122.7 (bpy–C), 117.6 (Ph–C), 116.8 (Ph–C).

MS (ESI+; MeOH): *m/z* (%) = 647.1 (100) $[M+H]^+$.

UV-vis (1:1 aqueous HOTf (0.10 M, pH 1.0) and TFE): λ [nm] (ε $[M^{-1}cm^{-1}]$) = 329 (3.3×10^4), 382 (1.6×10^4), 490 (br, 0.4×10^4), 561 (0.4×10^4).

Synthesis of complex 2

A suspension of $\mathbf{H_2L^2}$ (300 mg, 0.76 mmol), $RuCl_2(dmso)_4$ (300 mg, 0.61 mmol) and NEt_3 (0.5 mL) in degassed methanol (50 mL) was heated to reflux for 7 h. Pyridine (1.2 mL, 15 mmol) was then added and the reaction mixture was heated at 80 °C overnight. After cooling to rt, the solvent was removed under reduced pressure and the product was purified by column chromatography (DCM/MeOH 100:1); complex **2** was obtained in 10% yield as a brown solid.

^{1}H-NMR (500.3 MHz, MeOH-d_4): δ [ppm] = 10.03 (dd, J = 8.0, 1.4 Hz, 1H, Ar–H), 8.93 (dd, J = 4.7, 1.4 Hz, 1H, Ar–H), 8.69 (d, J = 8.0 Hz, 1H, bpy–H), 8.66 (d, J = 8.0 Hz, 1H, bpy–H), 8.52 (dd, J = 5.0, 1.4 Hz, 1H, Ar–H), 8.40 (d, J = 7.8 Hz, 1H, bpy–H), 8.31 (d, J = 7.8 Hz, 1H, bpy–H), 8.01–8.11 (m, 7H, py, bpy, Ar–H), 7.71 (dd, J = 7.9, 4.9 Hz, 1H, Ar–H), 7.45 (dd, J = 8.0, 4.6 Hz, 1H, Ar–H), 7.33 (tt, J = 7.6, 1.5 Hz, 2H, py–H), 6.81 (m, 4H, py–H).

^{13}C-NMR (125.8 MHz, MeOH-d_4): δ [ppm] = 162.9 (1 C, imidazole–C), 161.5 (1 C, bpy–C), 161.5 (1 C, imidazole–C), 161.5 (1 C, bpy–C), 156.5 (2 C, bpy–C), 156.3 (1 C, imidazole, Ar–C), 154.8 (1 C, imidazole, Ar–C), 153.3 (4 C, py–C), 147.9 (1 C, Ar–C), 144.0 (1 C, Ar–C), 138.0 (2 C, py–C), 137.8 (1 C, imidazole, Ar–C), 136.0 (1 C, Ar–C), 135.3 (1 C, bpy–C), 135.2 (1 C, bpy–C), 127.9 (1 C, Ar–C), 125.9 (4 C, py–C), 125.7 (1 C, Ar–C), 124.6 (1 C, bpy–C), 124.5 (1 C, bpy–C), 123.7 (1 C, bpy–C), 122.9 (1 C, bpy–C), 120.3 (1 C, Ar–C), 119.9 (1 C, Ar–C).

^{15}N-NMR (50.7 MHz, MeOH-d_4): δ [ppm] = −196.0 (1 N, imidazole–N), −137.4 (2 N, py–N), −125.5 (1 N, Ar–N), −101.8 (1 N, bpy–N), −100.6 (1 N, Ar–N), −99.1 (1 N, bpy–N).

MS (ESI+; MeOH): *m/z* (%) = 649.2 (100) $[M+H]^+$.

UV-vis (1: 1 aqueous HOTf (0.10 M, pH 1.0) and TFE): λ [nm] (ε $[M^{-1}cm^{-1}]$) = 331 (3.4×10^4), 374 (1.7×10^4), 430 (0.6×10^4), 497 (br, 0.3×10^4), 561 (br, 0.2×10^4).

Synthesis of singly protonated complex [1H]PF_6

A solution of complex **1** (5 mg, 0.007 mmol) in CH_2Cl_2 (3 mL) was treated with aqueous HPF_6 (~55 wt.% in H_2O, 3 μL, 0.03 mmol) and the reaction mixture was stirred for 1 h at rt. The solvent was then evaporated and the residue dissolved in MeOH. Single crystals suitable for X-ray diffraction were obtained by slow diffusion of diethyl ether into the solution of [**1**H]PF_6 in MeOH.

Synthesis of doubly protonated omplex [1H_2](CF_3SO_3)$_2$

Aqueous trifluoromethanesulfonic acid (0.66 M, 45 μL, 0.031 mmol) was added to a solution of **1** (5 mg, 0.007 mmol) in CH_2Cl_2. After stirring for 1 h at rt, the solvent was removed and the product was dried under vacuum. Crystalline material was obtained by slow diffusion of diethyl ether into a solution of [**1**H_2](CF_3SO_3)$_2$ in MeOH.

^{1}H-NMR (600.3 MHz, MeOH-d_4): δ [ppm] = 8.83 (d, J = 8.3 Hz, 2H, Ar–H), 8.77 (dd, J = 8.1, 1.0 Hz, 2H, bpy–H), 8.42 (dd, J = 7.9, 0.9 Hz, 2H, bpy–H), 8.23 (t, J = 8.0 Hz, 2H, bpy–H), 7.95 (m, 4H, py–H), 7.92 (ddd, J = 8.3, 7.2, 1.2 Hz, 2H, Ar–H), 7.81 (d, J = 8.2 Hz, 2H, Ar–H), 7.71 (ddd, J = 8.1, 7.1, 1.0 Hz, 2H, Ar–H), 7.48 (tt, J = 7.6, 1.5 Hz, 2H, py–H), 6.96 (m, 4H, py–H).

^{13}C-NMR (125.8 MHz, MeOH-d_4): δ [ppm] = 161.6 (bpy–C), 153.5 (bpy–C), 153.3 (py–C), 141.4 (Ar–C), 138.8 (py–C), 137.0 (bpy–C), 127.7 (Ar–C), 127.4 (Ar–C), 126.6 (py–C), 125.7 (bpy–C), 124.2 (bpy–C), 122.9, 120.3, 118.0 (Ar–C), 115.1 (Ar–C).

UV-vis (MeOH): λ [nm] (ε $[M^{-1}cm^{-1}]$) = 320 (3.5×10^4), 356 (2.1×10^4), 408 (0.5×10^4), 480 (br, 0.4×10^4).

Synthesis of Complex [2H_2](CF_3SO_3)$_2$

Aqueous trifluoromethanesulfonic acid (0.66 M, 45 μL, 0.031 mmol) was added to a solution of **2** (5 mg, 0.007 mmol) in CH_2Cl_2 (2 m), After stirring for 1 h at rt, the solvent was removed and the product was dried under vacuum.

^{1}H-NMR (400.3 MHz, MeOH-d_4): δ [ppm] = 10.17 (dd, J = 8.1, 1.3 Hz, 1H, Ar–H), 9.20 (dd, J = 4.7, 1.5 Hz, 1H, Ar–H), 8.83 (m, 2H, bpy–H), 8.66 (dd, J = 5.4, 1.3 Hz, 1H, Ar–H), 8.50 (d, J = 8.0 Hz, 1H, bpy–H), 8.46 (d, J = 8.1 Hz, 1H, bpy–H), 8.20–8.27 (m, 3H, bpy, Ar–H), 8.05 (m, 4H, py–H), 7.99 (dd, J = 8.1, 5.4 Hz, 1H, Ar–H), 7.77 (dd, J = 8.2, 4.7 Hz, 1H, Ar–H), 7.45 (tt, J = 7.6, 1.6 Hz, 2H, py–H), 6.93 (m, 4H, py–H).

^{13}C-NMR (100.7 MHz, MeOH-d_4): δ [ppm] = 162.7 (1 C, imidazole–C), 162.0 (1 C, bpy–C), 161.6 (1 C, bpy–C), 156.2 (1 C, imidazole–C), 154.9 (1 C, bpy–C), 153.3 (1 C, imidazole, Ar–C), 153.2 (5 C, py, bpy–C), 150.3 (2 C, imidazole, Ar–C), 141.8 (1 C, Ar–C), 138.8 (2 C, py–C), 138.4 (1 C, imidazole, Ar–C), 136.8 (1 C, bpy–C), 136.3 (1 C, bpy–C), 130.7 (1 C, Ar–C), 128.9 (1 C, imidazole, Ar–C), 126.5 (4 C, py–C), 126.4 (1 C, bpy–C), 126.3 (1 C, bpy–C), 125.1 (1 C, bpy–C), 124.8 (1 C, bpy–C), 123.9 (1 C, Ar–C), 123.0 (1 C, Ar–C), 121.1 (1 C, Ar–C).

^{15}N-NMR (40.6 MHz, MeOH-d_4): δ [ppm] = −231.0 (1 N, imidazole–N), −194.3 (1 N, imidazole–N), −158.4 (1 N, Ar–N), −142.6 (2 N, py–N), −101.4 (1 N, bpy–N), −99.6 (1 N, bpy–N), −97.3 (1 N, Ar–N).

UV-vis (MeOH): λ [nm] (ε $[M^{-1}cm^{-1}]$) = 325 (3.6×10^4), 356 (1.7×10^4), 487 (br, 0.3×10^4).

X-ray crystallography

Crystal data and details of the data collections are provided in the Supporting Information (see Table A1).

Deposition Numbers 2206588 (for **1**), 2206589 (for [**1**H]PF_6), and 2206590 (for [**1**H_2]$(CF_3SO_3)_2$) contain the supplementary crystallographic data for this paper. These data are provided free of charge by the joint Cambridge Crystallographic Data Centre and Fachinformationszentrum Karlsruhe Access Structures service www.ccdc.cam.ac.uk/structures.

Acknowledgements

*This project has been funded by the Deutsche Forschungsgemeinschaft (DFG, German Research Foundation) project 217133147 (SFB 1073, project C01). Purchase of the computer cluster (used for the calculation of the structure model of **2**) and of the X-ray diffractometer was supported by DFG projects 405832858 (INST 186/1294-1 FUGG) and 423268549 (INST 186/1327-1 FUGG), respectively, and by the Nds. Ministerium für Wissenschaft und Kultur (MWK). Open Access funding enabled and organized by Projekt DEAL.*

Conflict of Interest

The authors declare no conflict of interest.

Data Availability Statement

The data that support the findings of this study are available from the corresponding author upon reasonable request.

Keywords: Mechanistic studies · N-donor ligands · NMR spectroscopy · Ruthenium · Water oxidation catalysis

[1] J. Barber, *Chem. Soc. Rev.* **2009**, *38*, 185–196.
[2] S. Berardi, S. Drouet, L. Francàs, C. Gimbert-Suriñach, M. Guttentag, C. Richmond, T. Stoll, A. Llobet, *Chem. Soc. Rev.* **2014**, *43*, 7501–7519.
[3] H. Dau, I. Zaharieva, *Acc. Chem. Res.* **2009**, *42*, 1861–1870.
[4] K. S. Joya, H. J. M. de Groot, *ChemSusChem* **2014**, *7*, 73–76.
[5] N. S. Lewis, D. G. Nocera, *PNAS* **2006**, *103*, 15729–15735.
[6] W. Song, Z. Chen, M. K. Brennaman, J. J. Concepcion, A. O. T. Patrocinio, N. Y. Murakami Iha, T. J. Meyer, *Pure Appl. Chem.* **2011**, *83*, 749–768.
[7] M. D. Kärkäs, E. V. Johnston, O. Verho, B. Akermark, *Acc. Chem. Res.* **2014**, *47*, 100–111.
[8] V. Balzani, S. Campagna, Eds, *Photochemistry and Photophysics of Coordination Compounds I;* Springer Berlin Heidelberg, Berlin, Heidelberg, **2007**.
[9] S. Campagna, F. Puntoriero, F. Nastasi, G. Bergamini, V. Balzani in *Photochemistry and Photophysics of Coordination Compounds I, Topics in Current Chemistry*; (Eds. V. Balzani, S. Campagna), Springer Berlin Heidelberg, Berlin, Heidelberg, **2007**, pp. 117–214.
[10] J. J. Concepcion, J. W. Jurss, J. L. Templeton, T. J. Meyer, *J. Am. Chem. Soc.* **2008**, *130*, 16462–16463.
[11] D. G. H. Hetterscheid, J. N. H. Reek, *Angew. Chem. Int. Ed.* **2012**, *51*, 9740–9747; *Angew. Chem.* **2012**, *124*, 9878–9885.
[12] R. Matheu, M. Z. Ertem, J. Benet-Buchholz, E. Coronado, V. S. Batista, X. Sala, A. Llobet, *J. Am. Chem. Soc.* **2015**, *137*, 10786–10795.
[13] R. Matheu, P. Garrido-Barros, M. Gil-Sepulcre, M. Z. Ertem, X. Sala, C. Gimbert-Suriñach, A. Llobet, *Nat. Chem. Rev.* **2019**, *3*, 331–341.
[14] C. Sens, I. Romero, M. Rodríguez, A. Llobet, T. Parella, J. Benet-Buchholz, *J. Am. Chem. Soc.* **2004**, *126*, 7798–7799.
[15] R. Zong, R. P. Thummel, *J. Am. Chem. Soc.* **2005**, *127*, 12802–12803.
[16] F. Bozoglian, S. Romain, M. Z. Ertem, T. K. Todorova, C. Sens, J. Mola, M. Rodríguez, I. Romero, J. Benet-Buchholz, X. Fontrodona, C. J. Cramer, L. Gagliardi, A. Llobet, *J. Am. Chem. Soc.* **2009**, *131*, 15176–15187.
[17] S. Neudeck, S. Maji, I. López, S. Meyer, F. Meyer, A. Llobet, *J. Am. Chem. Soc.* **2014**, *136*, 24–27.
[18] D. W. Shaffer, Y. Xie, J. J. Concepcion, *Chem. Soc. Rev.* **2017**, *46*, 6170–6193.
[19] M. Z. Ertem, J. J. Concepcion, *Inorg. Chem.* **2020**, *59*, 5966–5974.
[20] L. Duan, F. Bozoglian, S. Mandal, B. Stewart, T. Privalov, A. Llobet, L. Sun, *Nat. Chem.* **2012**, *4*, 418–423.
[21] B. Zhang, L. Sun, *J. Am. Chem. Soc.* **2019**, *141*, 5565–5580.
[22] L. Wang, L. Duan, Y. Wang, M. S. G. Ahlquist, L. Sun, *Chem. Commun.* **2014**, *50*, 12947–12950.
[23] L. Duan, C. M. Araujo, M. S. G. Ahlquist, L. Sun, *PNAS* **2012**, *109*, 15584–15588.
[24] J. T. Muckerman, M. Kowalczyk, Y. M. Badiei, D. E. Polyansky, J. J. Concepcion, R. Zong, R. P. Thummel, E. Fujita, *Inorg. Chem.* **2014**, *53*, 6904–6913.
[25] L. Duan, A. Fischer, Y. Xu, L. Sun, *J. Am. Chem. Soc.* **2009**, *131*, 10397–10399.
[26] G. Zhang, R. Zong, H.-W. Tseng, R. P. Thummel, *Inorg. Chem.* **2008**, *47*, 990–998.
[27] J. Creus, R. Matheu, I. Peñafiel, D. Moonshiram, P. Blondeau, J. Benet-Buchholz, J. García-Antón, X. Sala, C. Godard, A. Llobet, *Angew. Chem. Int. Ed.* **2016**, *128*, 15608–15612.
[28] L. Duan, L. Wang, F. Li, F. Li, L. Sun, *Acc. Chem. Res.* **2015**, *48*, 2084–2096.
[29] S. Zhan, D. Mårtensson, M. Purg, S. C. L. Kamerlin, M. S. G. Ahlquist, *Angew. Chem. Int. Ed.* **2017**, *56*, 6962–6965; *Angew. Chem.* **2017**, *129*, 7066–7069.
[30] J. J. Concepcion, J. W. Jurss, P. G. Hoertz, T. J. Meyer, *Angew. Chem. Int. Ed.* **2009**, *48*, 9473–9476; *Angew. Chem.* **2009**, *121*, 9637–9640.
[31] F. Li, B. Zhang, X. Li, Y. Jiang, L. Chen, Y. Li, L. Sun, *Angew. Chem. Int. Ed.* **2011**, *50*, 12276–12279; *Angew. Chem.* **2011**, *123*, 12484–12487.
[32] F. Liu, T. Cardolaccia, B. J. Hornstein, J. R. Schoonover, T. J. Meyer, *J. Am. Chem. Soc.* **2007**, *129*, 2446–2447.
[33] F. Niu, D. Wang, F. Li, Y. Liu, S. Shen, T. J. Meyer, *Adv. Energy Mater.* **2020**, *10*, 1900399.
[34] D. Schindler, M. Gil-Sepulcre, J. O. Lindner, V. Stepanenko, D. Moonshiram, A. Llobet, F. Würthner, *Adv. Energy Mater.* **2020**, *10*, 2002329.
[35] M. A. Hoque, M. Gil-Sepulcre, A. de Aguirre, J. A. A. W. Elemans, D. Moonshiram, R. Matheu, Y. Shi, J. Benet-Buchholz, X. Sala, M. Malfois, E. Solano, J. Lim, A. Garzón-Manjón, C. Scheu, M. Lanza, F. Maseras, C. Gimbert-Suriñach, A. Llobet, *Nat. Chem.* **2020**, *12*, 1060–1066.
[36] R. Matheu, L. Francàs, P. Chernev, M. Z. Ertem, V. Batista, M. Haumann, X. Sala, A. Llobet, *ACS Catal.* **2015**, *5*, 3422–3429.
[37] Y. Liu, S.-M. Ng, S.-M. Yiu, W. W. Y. Lam, X.-G. Wei, K.-C. Lau, T.-C. Lau, *Angew. Chem. Int. Ed.* **2014**, *53*, 14468–14471; *Angew. Chem.* **2014**, *126*, 14696–14699.
[38] R. Zong, R. P. Thummel, *J. Am. Chem. Soc.* **2004**, *126*, 10800–10801.
[39] Y. Pineda-Galvan, A. K. Ravari, S. Shmakov, L. Lifshits, N. Kaveevivitchai, R. Thummel, Y. Pushkar, *J. Catal.* **2019**, *375*, 1–7.
[40] S. Dutta, S. Baitalik, M. Ghosh, U. Flörke, K. Nag, *Inorg. Chim. Acta* **2011**, *372*, 227–236.
[41] K. Mizushima, M. Nakaura, S.-B. Park, H. Nishiyama, H. Monjushiro, K. Harada, M. Haga, *Inorg. Chim. Acta* **1997**, *261*, 175–180.
[42] A. Enthart, J. C. Freudenberger, J. Furrer, H. Kessler, B. Luy, *J. Magn. Reson.* **2008**, *192*, 314–322.
[43] B. Luy, K. Kobzar, H. Kessler, *Angew. Chem. Int. Ed.* **2004**, *43*, 1092–1094; *Angew. Chem.* **2004**, *116*, 1112–1115.
[44] A.-C. Pöppler, H. Keil, D. Stalke, M. John, *Angew. Chem. Int. Ed.* **2012**, *51*, 7843–7846; *Angew. Chem.* **2012**, *124*, 7963–7967.
[45] A. Navarro-Vázquez, *Magn. Reson. Chem.* **2012**, *50*, S73–9.
[46] Gaussian 16, Revision A.03, M. J. Frisch, G. W. Trucks, H. B. Schlegel, G. E. Scuseria, M. A. Robb, J. G. Cheeseman, G. Scalmani, V. Barone, G. A. Petersson, H. Nakatsuji, X. Li, M. Caricato, A. V. Marenich, J. Blonio, B. G. Janesko, R. Gomperts, B. Mennucci, H. P. Hratchian, J. V. Ortiz, A. F. Izmaylov, J. L. Sonnenberg, B. Williams-Young, F. Ding, F. Lipparini, F. Egidi, J. Goings, B. Peng, A. Petrone, T. Henderson, D. Ranasinghe, V. G. Zakrzewski, J. Gao, N. Rega, G. Zheng, W. Liang, M. Hada, M. Ehara, K. Toyota, R. Fukuda, J. Hasegawa, M. Ishida, T. Nakajima, Y. Honda, O.

Research Article
doi.org/10.1002/ejic.202200597

Kitao, H. Nakai, T. Vreven, K. Thorossell, J. A. Montgomery Jr, J. E. Peralta, F. Ogliaro, M. J. Bearpark, J. J. Heyd, E. N. Brothers, K. N. Kudin, V. N. Staroverov, T. A. Keith, R. Kobayashi, J. Normand, K. Raghavachari, A. P. Rendell, J. C. Burant, S. S. Iyengar, J. Tomasi, M. Cossi, J. M. Millam, M. Klene, C. Adamo, R. Cammi, J. W. Ochterski, R. L. Martin, K. Morokuma, O. Farkas, J. B. Foresman, D. J. Fox, Gaussian, Inc, Wallingford CT, **2016**.

[47] G. Cornilescu, J. L. Marquardt, M. Ottiger, A. Bax, *J. Am. Chem. Soc.* **1998**, *120*, 6836–6837.

[48] S. Neudeck, S. Maji, I. López, S. Dechert, J. Benet-Buchholz, A. Llobet, F. Meyer, *Inorg. Chem.* **2016**, *55*, 2508–2521.

[49] K. Okamoto, J. Miyawaki, K. Nagai, D. Matsumura, A. Nojima, T. Yokoyama, H. Kondoh, T. Ohta, *Inorg. Chem.* **2003**, *42*, 8682–8689.

[50] A. C. Sander, S. Maji, L. Francàs, T. Böhnisch, S. Dechert, A. Llobet, F. Meyer, *ChemSusChem* **2015**, *8*, 1697–1702.

[51] D. J. Wasylenko, C. Ganesamoorthy, B. D. Koivisto, M. A. Henderson, C. P. Berlinguette, *Inorg. Chem.* **2010**, *49*, 2202–2209.

[52] M. Gil-Sepulcre, M. Böhler, M. Schilling, F. Bozoglian, C. Bachmann, D. Scherrer, T. Fox, B. Spingler, C. Gimbert-Suriñach, R. Alberto, R. Bofill, X. Sala, S. Luber, C. J. Richmond, A. Llobet, *ChemSusChem* **2017**, *10*, 4517–4525.

[53] A. Ghosh, S. Dasgupta, A. Kundu, S. Mandal, *Dalton Trans.* **2022**, *51*, 10320–10337.

[54] I. P. Evans, A. Spencer, G. Wilkinson, *J. Chem. Soc, Dalton Trans.* **1973**, 204.

Manuscript received: September 22, 2022
Revised manuscript received: November 7, 2022
Accepted manuscript online: November 17, 2022